Supporting Information

Synergistic electronic modulation and Cl^- shielding of Fe sites for robust seawater electrolysis

Hao Wang[a+], Pengwu Jiang[b+], Nannan Jiang[a], Weili Zhang[b], Bing Huang*[b], Xuwei Liu[a], Huihui Jin[a], and Lunhui Guan*[a]

[a] State Key Laboratory of Structural Chemistry, Fujian Key Laboratory of Nanomaterials, Fujian Institute of Research on the Structure of Matter, Chinese Academy of Sciences, Fuzhou, Fujian 350002, China.

[b] Division of Biobased Chemicals, Institute of Zhejiang University-Quzhou, Quzhou 324000, P.R. China.

[+] These authors contributed equally: Hao Wang, Pengwu Jiang

* Corresponding authors at: State Key Laboratory of Structural Chemistry, Fujian Key Laboratory of Nanomaterials, Fujian Institute of Research on the Structure of Matter, Chinese Academy of Sciences, Fuzhou, Fujian 350002, China.

E-mail address: huangbing@zju-qz.edu.cn (B. Huang), guanlh@fjirsm.ac.cn (L. Guan)

Keywords: electrochemical catalysis, oxygen evolution reaction, seawater electrolysis, membrane electrode assembly, anion exchange membrane electrolyzer

Supporting note 1：

AEMWE measurement

The Ce-NiFeOOH/PO_4^{3-} catalyst was sprayed over Ni fibers and carbon paper, forming electrodes (2 cm^2) that were integrated into an anion exchange membrane (AEM) water electrolysis cell. The anode and cathode were separated using an anion exchange membrane (Sustainion® X37-50-grade T, America). The catalytic AEM cell's performance was evaluated with a power supply (Interface 5000E, Gamry) and 1.0 M KOH + seawater fed in at a flow rate of 60 mL min^{-1}. Voltage and current measurements provided information on the cell's operational efficiency.

Electrolyzer efficiency

H_2 production rate @ 0.5 A cm^{-2}

$= (j \text{ A cm}^{-2})(1 \text{ e}^-/1.602 \times 10^{-19} \text{ C})(1 \text{ H}_2/2 \text{ e}^-)$

$= 0.5 \text{ A cm}^{-2} / (1.602 \times 10^{-19} \text{ C x } 2)$

$= 2.59 \times 10^{-6} \text{ mol H}_2 \text{ cm}^{-2} \text{ s}^{-1}$

LHV of H_2

$= 120 \text{ kJ g}^{-1} \text{ H}_2 = 2.42 \times 10^5 \text{ J mol}^{-1} \text{ H}_2$

H_2 power out

$= (2.59 \times 10^{-6} \text{ mol cm}^{-2} \text{ s}^{-1}) \times (2.42 \times 10^5 \text{ J mol}^{-1})$

$= 0.627 \text{ W cm}^{-2}$

Electrolyzer Power of Ce-NiFeP||Pt/C

Electrolyzer Power (Ce-NiFeP) @ 0.5 A cm^{-2}

= (0.5 A cm^{-2}) (1.68 V)

= 0.84 W cm^{-2}

Efficiency of Ce-NiFeP||Pt/C

= (H_2 Power Out) / (Electrolyzer Power)

= 0.627 W cm^{-2}/0.84 W cm^{-2}

= 74.6%

Price per gasoline-gallon equivalent (GGE)H_2 @0.5A cm^{-2}

= 1GGE H_2 / H_2 production rate × Electrolyzer power × Electricity bill

= 0.997 kg/(2.59 × 10^{-6} mol H_2.cm^{-2} s^{-1} × 2 kg/mol) × 0.84 W cm^{-2} × \$ 0.02/kWh

= \$ 0.90/GGE H_2

Calculation of basic electricity expense for H_2 production [1]

The total electricity consumption for H_2 production was calculated according to the following equation:

$$W = I \times \int U\,dt \qquad (1)$$

Where the W is the total electricity consumption, I is the electrolyzer current, U is the electrolyzer voltage, and t is the reaction time.

The amount of H, generation was calculated based on the following equation:

$$V = 22.4 \times I \times t / (Z \times F) \qquad (2)$$

Where V is the volume of produced H_2, Z is the electron transfer number (the value of 2 for HER), and F is the Faraday constant (96485 $Cmol^{-1}$).

According to the above results, the basic electricity expense for H_2 production was calculated as:

$$Q = W / V \ (kWh\ m^{-3}\ H_2) \qquad (3)$$

For an ideal catalyst, assuming that it has no performance decay during the stability test of water splitting, the calculation of basic electricity expense for H_2 production can be simplified to the formula [$Q = 2.39 \times U$ ($kWh\ m^{-3}\ H_2$)] according to the Eqs. (1-3).

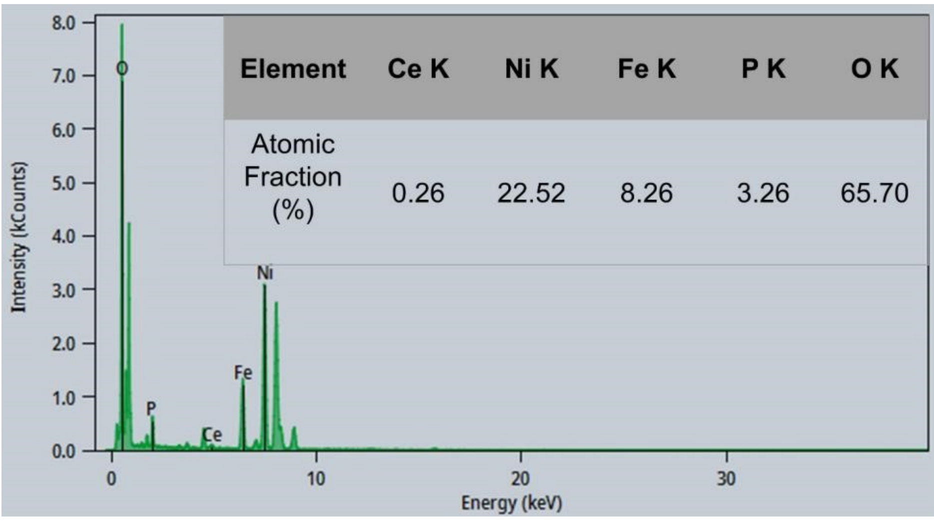

Element	Ce K	Ni K	Fe K	P K	O K
Atomic Fraction (%)	0.26	22.52	8.26	3.26	65.70

Figure S1. Detailed parameters for TEM EDS of Ce-Ni(Fe)OOH/PO_4^{3-}.

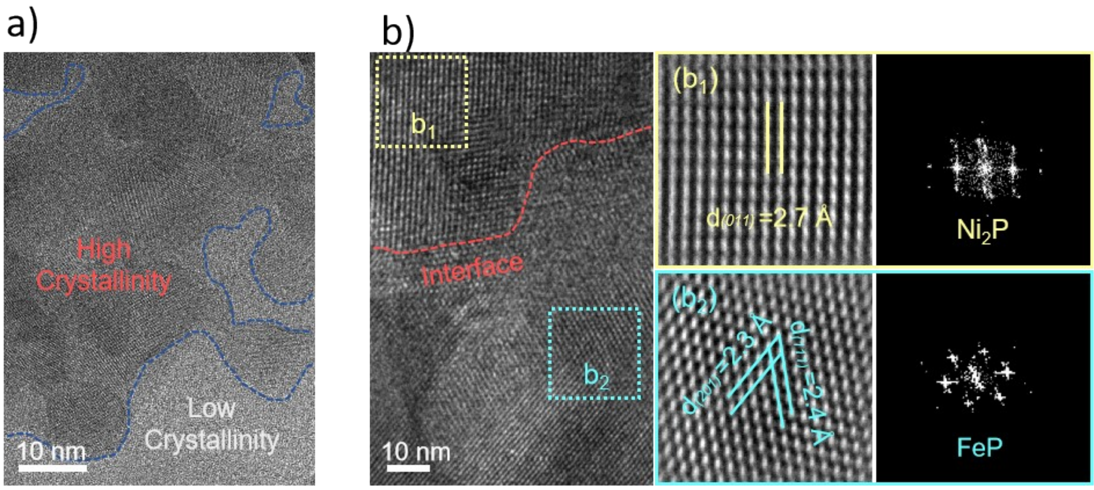

Figure S2. (a) The HR-TEM images of Ce-NiFeP. (b) The enlarged HRTEM image and corresponding Fourier transform pattern.

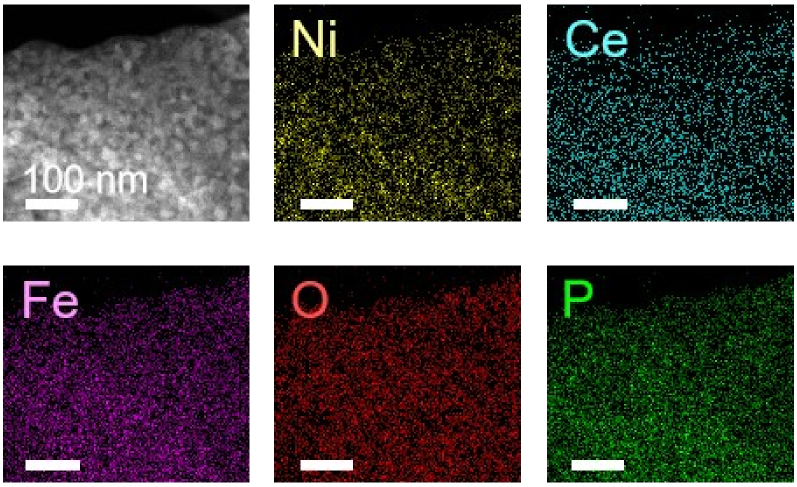

Figure S3. HAADF-STEM with EDS elemental mapping of Ce-NiFeP.

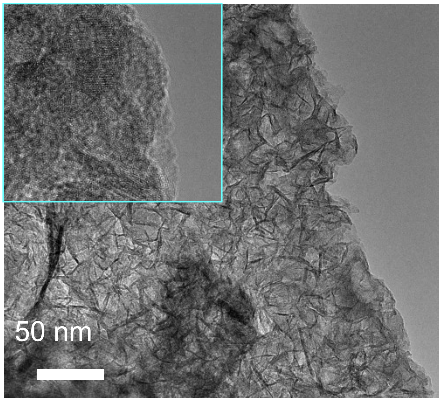

Figure S4. The TEM image of Ce-NiFeOOH/PO_4^{3-}.

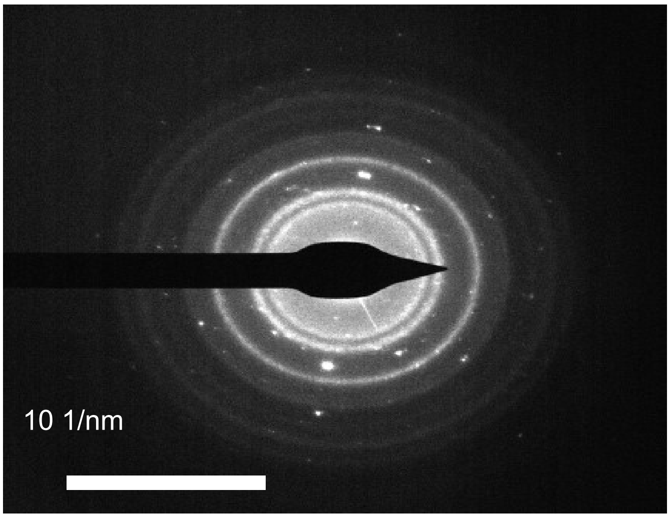

Figure S5. The SAED image of Ce-NiFeOOH/PO_4^{3-}.

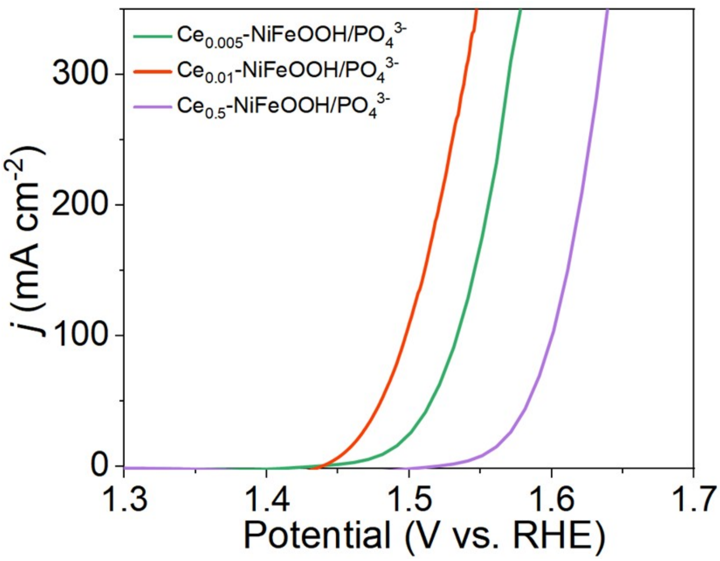

Figure S6. The LSV curves of of Ce-NiFeOOH/PO_4^{3-} with different Ce contents.

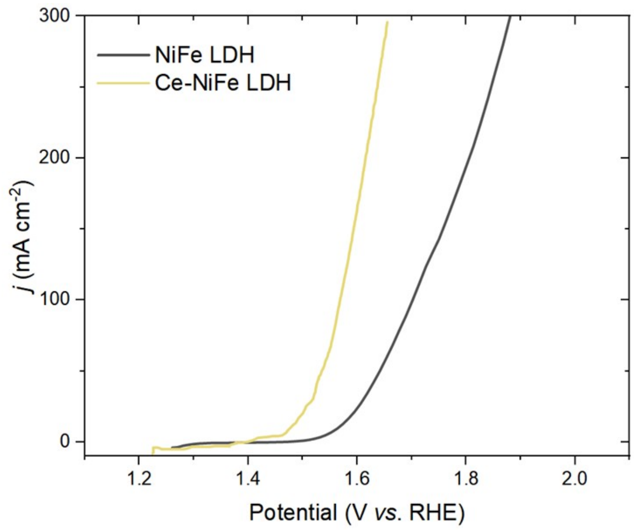

Figure S7. The LSV curves of Ce-NiFe LDH and NiFe LDH.

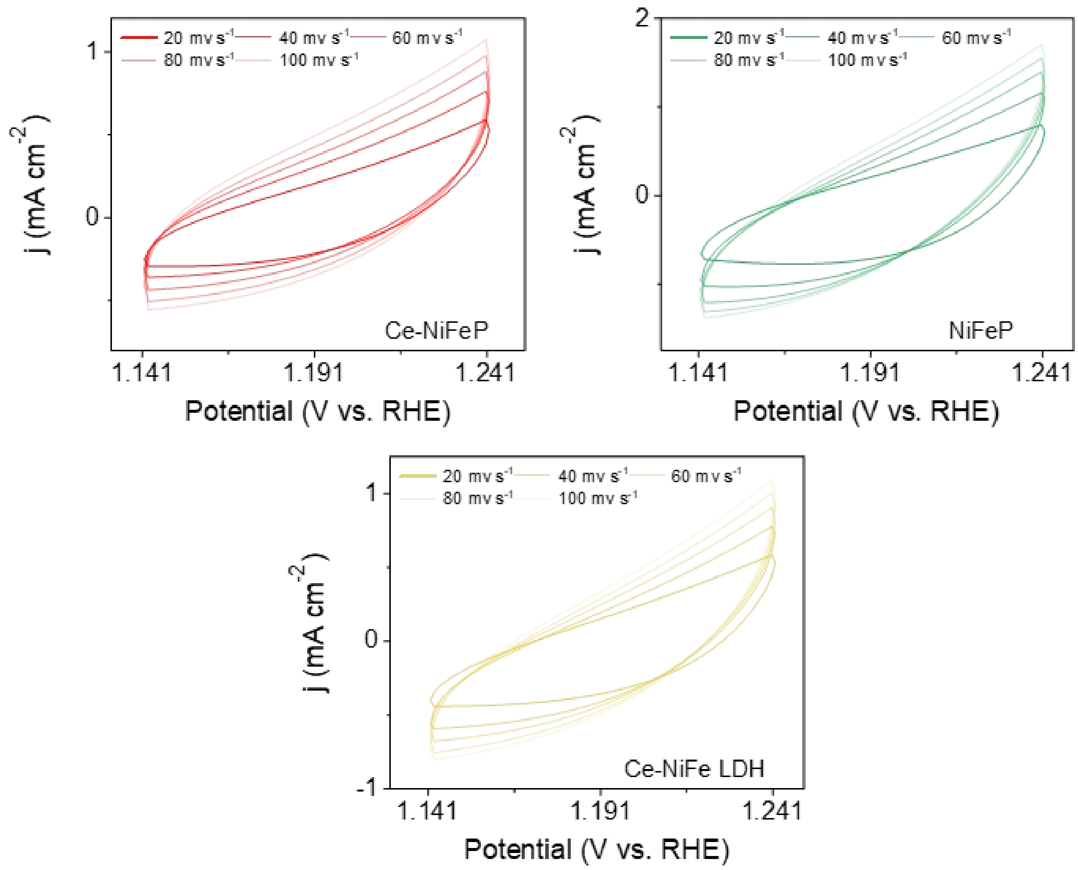

Figure S8. (a-c) CV curves of Ce-NiFeOOH/PO_4^{3-}, NiFeOOH and Ce-NiFe LDH electrodes.

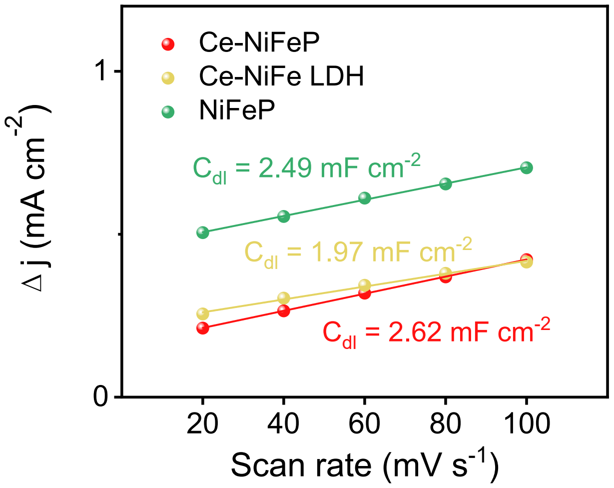

Figure S9. C_{dl} plots of Ce-NiFeOOH/PO_4^{3-}, NiFeOOH and Ce-NiFe LDH.

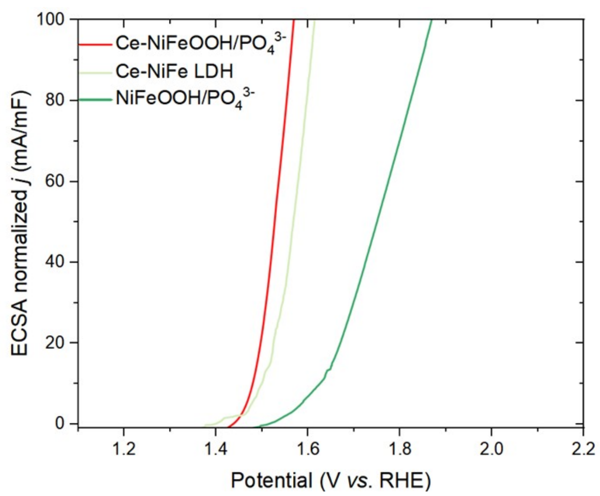

Figure S10. The ECSA normalized LSV curves of Ce-NiFeOOH/PO_4^{3-}, Ce-NiFe LDH, and NiFeOOH/PO_4^{3-}.

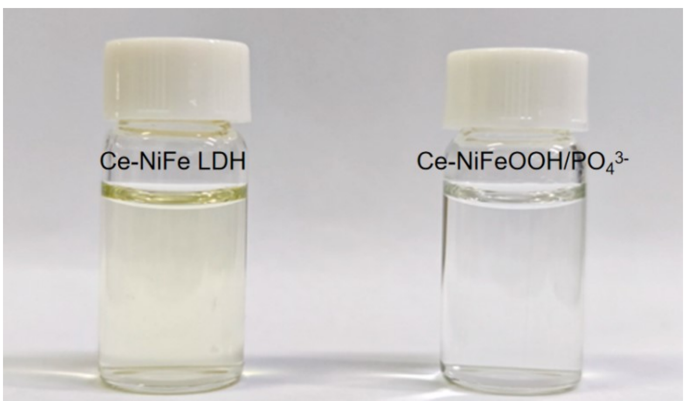

Figure S11. Optical image of ClO^- in the electrolyte after long-term stability testing of Ce-NiFe LDH and Ce-NiFeP in 1 M KOH + seawater, respectively.

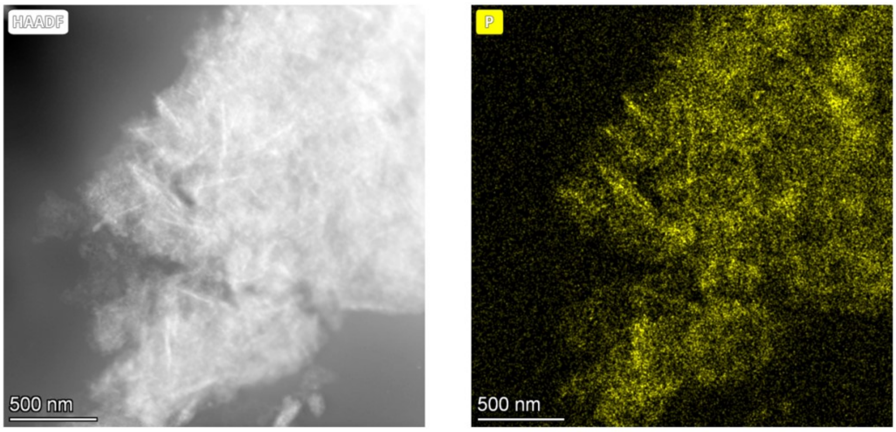

Figure S12. The HADDF-STEM and corresponding EDS mapping image of Ce-NiFeOOH/PO_4^{3-} after a 48-hour stability.

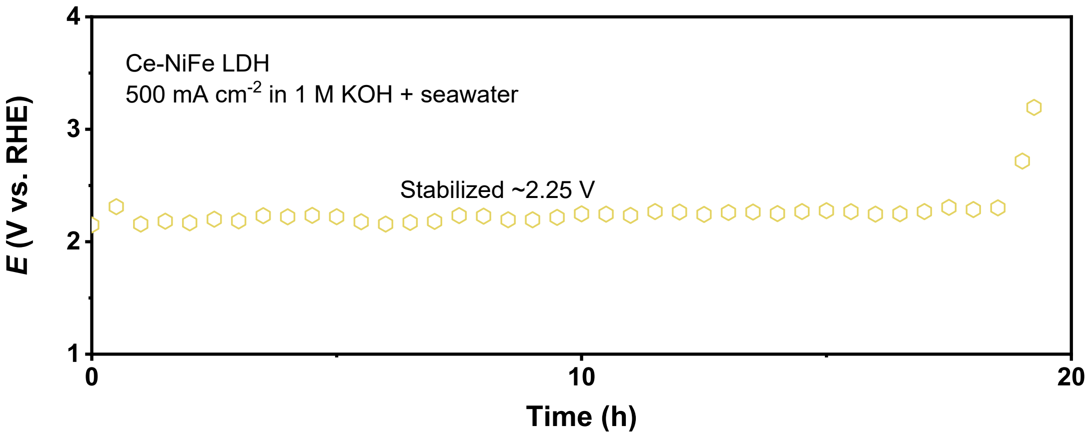

Figure S13. E-T curve of Ce-NiFe LDH in 1 M KOH + seawater electrolyte at 500 mA cm^{-2}.

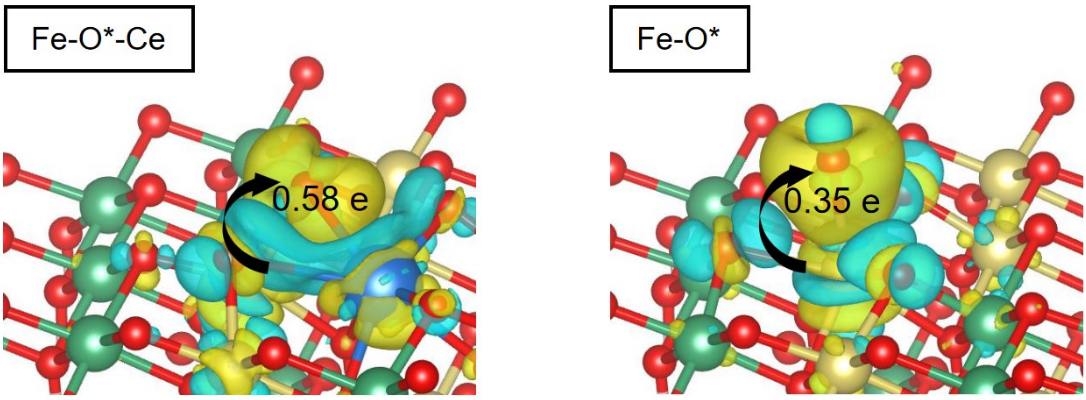

Figure S14. Charge density difference analysis.

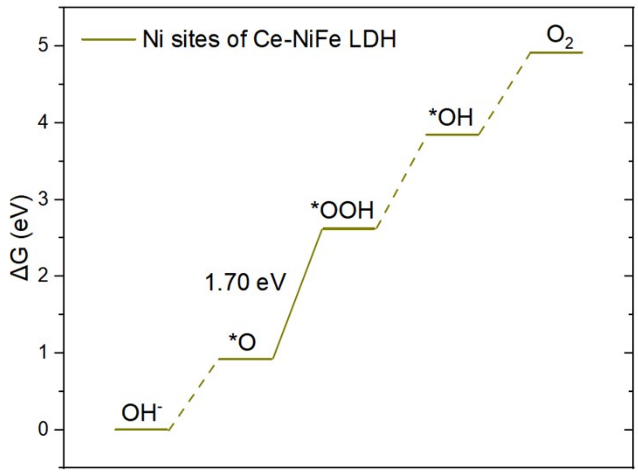

Figure S15. Free energy diagrams for OER on the Ni sites of Ce-Ni(Fe)OOH.

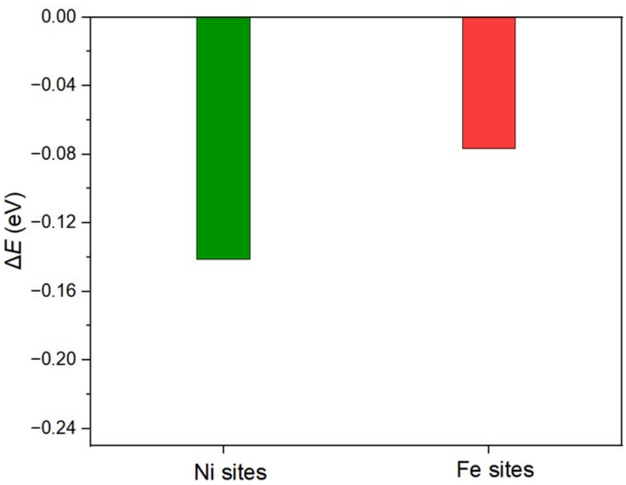

Figure S16. The adsorption energy of PO_4^{3-} on the Fe or Ni sites of Ce-Ni(Fe)OOH.

Table S1. Element analysis of Ce-NiFeP and NiFeP by ICP-OES.

	Ce-NiFeP			NiFeP	
Element	Ni	Fe	Ce	Ni	Fe
Element concentration (mg/L)	162.06	56.22	0.62	139.04	48.35
wt (%)	31.7	11.0	0.12	27.6	9.59

Table S2. Comparison of overpotentials of Ce-NiFeOOH/PO_4^{3-} at different current density in 1 M KOH, 1 M KOH + 0.5 M NaCl, and 1 M KOH + seawater, respectively.

Electrolyte	10 (mA cm^{-2})	100 (mA cm^{-2})	300 (mA cm^{-2})
1 M KOH	223	267	309
1 M KOH + 0.5 M NaCl	227	273	318
1 M KOH + seawater	230	286	348

Table S3. Comparison of $\eta_{@10\ mA\ cm^{-2}}$ in the reported literature for Ce-NiFeOOH/PO_4^{3-} in 1 M KOH.

Catalyst	$\eta_{@10\ mA\ cm-2}$ (mV)	Ref.
Ce-NiFeOOH/PO_4^{3-}	**223**	**This work**
MIL-88A/Ni(OH)(2)	250	2
$Co_4N@CeO_2$	263	3

$CoSe_2/MoSe_2$	320	4
R-$CoSeO_4$	265	5
3%IrO_x/NCNT	241	6
H-LSCF	240	7
Ni_3Fe-BDC	265	8
Fe_3O_4	270	9

Table S4. The calculated results for the free energy diagrams.

Free energies	Ce-Ni(Fe)OOH	Ni(Fe)OOH
M^*+2H_2O	0	0
$M^*OH+H_2O+H^+$	0.74	0.91
$M^*O+H_2O+2H^+$	2.48	2.34
$M^*OOH+3H^+$	3.57	3.96
$M^*+O_2+4H^+$	4.92	4.92

Table S5. Performance comparison of Ce-NiFeOOH/PO_4^{3-} with three other reported electrocatalysts in AEM seawater electrolyzers.

Catalyst	Co/P-Fe_3O_4	NFCP	$NiCoP_v$	Ce-NiFeOOH/PO_4^{3-}
Electrolyzer efficiency at 500 mA cm^{-2} (%)	68.5	59.9	51.6	74.6
Price per GGE H_2 at 500 mA cm^{-2} ($)	0.980	1.119	1.150	0.897
E at 500 mA cm^{-2} (V)	1.84	2.095	2.43	1.68
j_{max} (mA cm^{-2})	1000	500	900	1500
Electricity expense (kWh)	4.38	5.01	5.81	4.02

Ref.	*Appl. Catal. B: Environ.* **2024**, 357, 124269.	*ACS Catal.* **2024**,14,18322.	*Adv. Energy Mater*. **2024**, 14, 2400975	This work

References

1 D. Kong, C. Meng, Y. Wang, X. Chen, J. Zhang, L. Zhao, J. Ji, L. Zhang, Y. Zhou, High-density accessible Ru-O-Co moieties with accelerated formation of activated oxygen species for freshwater and seawater electrolysis, Appl. Catal. B: Environ., 2024, **343**, 123578.

2 Z. Qian, K. Wang, K. Shi, Z. Fu, Z. Mai, X. Wang, Z. Tang, Y. Tian, Interfacial electron transfer of heterostructured MIL-88A/Ni $(OH)_2$ enhances the oxygen evolution reaction in alkaline solutions, J. Mater. Chem. A, 2020, **8**, 3311-3321.

3 P. Zhou, G. Hai, G. Zhao, R. Li, X. Huang, Y. Lu, G. Wang, CeO_2 as an "electron pump" to boost the performance of Co_4N in electrocatalytic hydrogen evolution, oxygen evolution and biomass oxidation valorization, Appl. Catal. B: Environ., 2023, **325**, 122364.

4 Y. Yang, Y. Xiong, J. Yang, D. Qian, Y. Chen, Y. He, Z. Hu, Three-Dimensional Heterostructured $CoSe_2$/$MoSe_2$@CC as Trifunctional Electrocatalysts for Energy-Efficient Hydrogen Production, Energ. Fuels, 2024, **38**, 2260-2272.

5 J. Yu, W. Yu, Y. Wang, X. Li, R. Liu, X. Zhang, H. Liu, W. Zhou, Capture and recycling of toxic selenite anions by cobalt-based metal-organic-frameworks for electrocatalytic overall water splitting, Chem. Eng. J., 2022, **433**, 134553.

6 N. Liu, Y. Wang, Q. Zhang, J. Guan, Trifunctional iridium-based electrocatalysts for overall water splitting and Zn-air batteries, Electrochim. Acta, 2021, **380**, 138215.

7 H. Zhang, D. Guan, Z. Hu, Y. C. Huang, X. Wu, J. Dai, C. L. Dong, X. Xu, H. J. Lin, C. T. Chen, W. Zhou, Z. Shao, Exceptional lattice-oxygen participation on artificially controllable electrochemistry-induced crystalline-amorphous phase to boost oxygen-evolving performance, Appl. Catal. B: Environ., 2021, **297**, 120484.

8 L. Xiao, J. Han, Z. Wang, J. Guan, Nanorod-like NiFe metal-organic frameworks for oxygen evolution in alkaline seawater media, Int. J. Hydrogen Energy, 2023, **48**, 23776-23784.

9 N. Akbari, S. Nandy, K.H. Chae, M.M. Najafpour, Dynamic Changes of an Anodized FeNi Alloy during the Oxygen Evolution Reaction under Alkaline Conditions, Langmuir, 2023, **39**, 11807.